Article:
Hunter, TN, Peakall, J, Unsworth, TJ et al. (4 more authors) (2013) The influence of system scale on impinging jet sediment erosion: Observed using novel and standard measurement techniques. Chemical Engineering Research and Design, 91 (4). 742 - 734. ISSN 0263-8762

https://doi.org/10.1016/j.cherd.2013.02.002

Chemical Engineering Research & Design: Submission for special issue on Nuclear Process Engineering

The influence of system scale on impinging jet sediment erosion: observed using novel and standard measurement techniques

Timothy N. Hunter[1], Jeff Peakall[2], Thomas J. Unsworth[1], Mehmet Hakan Acun[1], Gareth Keevil[2], Hugh Rice[1], Simon Biggs[1]

[1] School of Process, Environmental and Materials Engineering, and [2] School of Earth and Environment, University of Leeds, U.K

Corresponding author: t.n.hunter@leeds.ac.uk

Abstract

Jet impingement as a method for eroding particulate beds and maintaining sediment in suspension is an important process for a host of industries, particularly in nuclear waste processing, where such systems to disperse and mix particulate beds have a number of advantages over other approaches. Existing work has utilised fairly rudimentary techniques for the measurement of erosion depths and here we demonstrate a new technique for measuring both static and dynamic erosion of cohesionless particulates under an impinging jet, using ultrasonic Doppler velocimetry. This approach is tested on both quartz sands and on a range of $Mg(OH)_2$ particulates that are key simulants for nuclear waste facilities, such as the Highly Active Storage Tanks at Sellafield, U.K. A critical jet height was found to exist that balanced the impingement velocities and total entrained jet volume to maximise erosion. The effect of system scale was also considered by normalising steady-state crater depths and sizes, with erosion being enhanced in the small scale, possibly due to increased turbulent recirculation. Additionally, velocity profiles and acoustic backscatter were used to determine both steady-state crater profiles and kinetic changes in bed-depths with time, and highlighted important differences between static and dynamic measurements of erosion depth.

Keywords: Impinging jets; Erosion; Ultrasonic velocity profiling; Cohesionless sediments; Scour

1 Introduction

The erosion of sediment beds due to interaction with turbulent liquid jets is important in the analysis of a number of hydraulic engineering and natural systems, such as scour from jetting in cooling or waste water pipe outlets and dredging operations (Yeh et al., 2009). Impinging liquid jets are also a convenient way to study the shear strength of sediment beds to understand the general erodibility of particulates (Debnath et al., 2007; Jain and Kothyari, 2009), and a number of papers report on the applied use of impinging jets as in situ cohesive strength devices (e.g. Al-Madhhachi et al., 2011; Caruso and Gabr, 2011; Tolhurst et al., 2000; Tolhurst et al., 2009).

The use of impinging jets is also common across many nuclear sites, particularly in the U.S. and U.K., as a means to disperse consolidated multiphase wastes (Hamm et al., 1989; McArthur et al., 2005; McArthur et al., 2012; Shekarriz and Hammad, 1997; Shekarriz et al., 1997). Jets are often preferred to mechanical mixers, due to their increased reliability in challenging environments. As such, they can be used both to maintain dispersion conditions and re-suspend settled sludges. Specifically at Sellafield in the U.K., jets are employed within the Highly Active Storage Tanks (HASTs) to disperse crystalline particulate fission products from leached Highly Active Liquor (HAL) wastes (Hunter et al., 2011a; McArthur et al., 2005). The particles are heat forming solids, and the jets are used to keep them in a mobile suspension to reduce the likelihood of hot-spot formation.

A greater understanding of the fundamental mechanisms of erosion is critical in many of these systems, and in particular, in nuclear facilities where online monitoring or other direct measurements are particularly challenging. Generally, erosion will be dependent on the properties of the fluid (density, viscosity), the physical properties of the bed material (size, shape, density) and the properties of the jet itself (velocity, flow regime and turbulence intensity). The dynamic flow forces acting on the particles will vary depending on the jet region. Within the impingement region, there will be competing forces of the jet pressure profile on the bed (analogous to a ‘compression’ type force normal to the bed) as well as the increasing influence of the jet shear forces on the bed, as it spreads out laterally. Further from the impingement zone, the jet expands as a radial wall jet, with erosion occurring from the interfacial shear-stress profile (Hogg et al., 1997; Kobus et al., 1979; Rajaratnam and Beltaos, 1977).

For cohesionless sediment (where minimal inter-particle adhesion exists) erosion is considered as single particle attrition, with a force balance between the particle and fluid averaged over the bed (Mazurek and Hossain, 2007). This allows at least a relative certainty in qualitative empirical assessment between different particle species. Nevertheless, the influence of turbulence and larger recirculation currents (Gioia and Bombardelli, 2005; Karim and Ali, 2000; Rajaratnam et al., 2010) leads to number of complexities and uncertainties that make quantitative analysis impossible in many cases (Xue et al., 2010).

An important issue is to what degree small-scale studies can be extended to larger-scale facilities. The ability to use small scale systems to evaluate performance has the advantages of much increased flexibility and associated faster data collection. However, the difficulty of scaling such

complex multiphase environments means any derived predictions must currently be made cautiously. There are a series of nominally scale-independent relationships derived from the study of sands and other cohesionless sediments (Aderibigbe and Rajaratnam, 1996) which promises some degree of normalisation between systems of different jet velocities, sizes and particulates. Hence here, using these relationships, we examine the scale-independence of jet impingement erosion dynamics in both quartz sands and $Mg(OH)_2$ particulates using a series of three experimental rigs of different scales.

Secondly, a key difficulty in past studies has been the measurement of dynamic scour depth, with workers using relatively rudimentary techniques, such as repeated measurements using a thin rod to identify the solid surface (Aderibigbe and Rajaratnam, 1996). More sophisticated techniques have been used such as acoustic Doppler velocimetry (ADV) yet this had to be placed off axis in order to be able to measure the base (Yeh et al., 2009). Measuring dynamic scour depth is hard because the surrounding medium is a highly turbulent particle-laden suspension that depending on concentration and grain properties may be opaque. Furthermore, the jet line is located directly above the point of maximum erosion making it difficult for instrumentation to access. Here we demonstrate a new non-intrusive methodology using ultrasonic velocity profiling (UVP), for measuring the dynamic scour depth at a frequency of up to 128 Hz, enabling both the maximum depth to be measured and the steady-state time-scale to be calculated. Such Doppler profilers are widely used for measuring flow in pipes and channels (Baas et al., 2009; Birkhofer et al., 2008; Harbottle et al., 2011; Kantoush et al., 2008; Kotze et al., 2011), assessing the performance of tank mixing systems (Ein-Mozaffari et al., 2007; Ein-Mozaffari and Upreti, 2009; Mali and Patwardhan, 2009), and can be used for analysing the consolidation of free-settling coagulated suspensions (Hunter et al., 2011b). However, this is the first study of impinging jet erosion dynamics using such instrumentation.

2 Experimental

2.1 Materials

Medium-grained sand (ρ_{s1} = 2643 kg/m^3), and magnesium hydroxide (Hydromag G®, ρ_{s2} = 2360 kg/m^3) in two size fractions supplied from the National Nuclear Laboratory, were used as cohesionless sediment bed materials in the erosion tests. Sand was chosen as a model particulate material for comparison with existing studies (e.g. Aderibigbe and Rajaratnam, 1996; Ansari et al., 2003; Kobus et al., 1979; Rajaratnam, 1982; Sequeiros et al., 2007; Yeh et al., 2009); while magnesium hydroxide was chosen as a general relevant simulant for the grain fractions of 'legacy' sludge wastes present in various U.K. nuclear waste stores (Hastings et al., 2007). Although the highly active fission particulates within the HASTs themselves may be generally finer (McArthur et

al., 2005), larger cohesionless materials were chosen to better allow the assessment of system scale and the performance of the ultrasonic velocity profiler. The particle size distributions were measured using a Malvern Mastersizer 2000 and are shown in Figure 1, while median (D_{50}) and 90th percentile (D_{90}) sizes are shown in Table 1. Due to the coarse magnesium hydroxide being partially outside of the size maximum for the Mastersizer (> 2,500 μm) the given D_{90} for this sediment was estimated using a 1000 – 2600 μm sieve mesh and microscopy.

The sand has a D_{50} of 328 μm and D_{90} of 489 μm, while the finer magnesium hydroxide has a slightly higher D_{50} (375 μm), but also a significantly increased proportion within the upper size fractions (with a relatively larger D_{90} of 702 μm). The 'coarse' magnesium hydroxide is markedly the largest of the particulates and one would expect therefore a lower level of erosion, based upon a model for the removal of single cohesionless particles. It is lastly noted that dissolution and re-precipitation of surface hydroxide ions in the magnesium hydroxide particles may produce an increase in yield strength and sediment cohesion over long time periods. Therefore, sediments were first left to equilibrate in the tank water for an hour (until a constant pH was monitored) and were left undisturbed in the tank for no longer than 24 hours. Additionally, all sediments were well mixed in the tanks and left for 15 minutes to settle before experiments were conducted to further reduce the likelihood of any build up in bed cohesion or compaction.

2.2 Visual analysis of erosion

Three different sized jet and tank systems were compared in erosion studies to assess the impact of changing system scale. The first was a small bench scale cylindrical tank with a diameter (d_t) of 280 mm and length of 400 mm (giving a fill volume of ~25 L). A 3 mm internal diameter jet line was used, with the jet driven by a variable speed peristaltic pump with water from a separate feed tank. The tank was completely filled with water and a flat sediment bed was created in the base of the tank with a thickness of ~40 mm. It is noted that at very high jet velocities, the bed was completely cleared from underneath the jet zone. A larger depth was not chosen however, as such limited bed depths approximate conditions within the HASTs. The jet-tip was set at various heights from 10 to 130 jet diameters (in respect to the original sediment bed interface). The variable speed pump allowed jet flow rates of 0.8 – 5.2 m/s (average tip velocities). The jet was run at each specific condition until a steady-state crater profile had been created, which normally occurred within 2 - 3 minutes. The final crater diameters created from given velocity and height conditions were quantified using Image J™ photo analysis software, where the sizes were measured to the crater peak. Image analysis of the change in crater size with time was initially used as a guide to determine how long the jet should be run to reach steady-state, where it was estimated to be

established if no measureable increase in crater diameter was recorded over 60 seconds. These steady-state times are generally smaller than have been previously reported by Aderibigbe and Rajaratnam (1996), and Ansari et al. (2003) however they are consistent with kinetic changes reported in other studies of sand by Yeh et al. (2011) and research in nuclear waste systems (McArthur et al., 2005; McArthur et al., 2012). Differences in the equilibrium times relative to some of the previously reported literature can be explained by considering that the erosion process will generally follow an exponential decay. Given this, there may be some possibility of continued erosion over very extended periods of time, however the steady-state as defined balanced the requirements for data collection and the macroscale detection limits of the visual analysis technique employed.

The final crater depths (ε) were measured using a graduated dip-stick that was lowered to just touch the crater base. The difference in the total distance measured with the graduated rule between the crater floor at the jet centre and original levelled bed was taken as the given depth measurement. All depth measurements taken this way were completed after the jet was turned off, and so represent static measurements. Although some previous literature exists comparing dynamic depths with the jet still initiated (Aderibigbe and Rajaratnam, 1996; Rajaratnam and Mazurek, 2003) the error in such measurement was deemed too high with this small jet system to be reliable, because of the fluid nature of the underlying bed from sediment recirculation. Other factors, such as the influence of any depth probes on the flow profile of the jet, were also considered to potentially lead to problems with any dynamic depth measurements taken this way.

Other similar experiments were conducted using the same 3 mm diameter jet and pump system, with a much larger 0.5 x 0.5 x 0.5 m tank (filled to a height of 400 mm, for a volume of 100 L), giving the ability to observe erosion differences when a much larger tank volume to jet diameter ratio was employed. Additionally, experiments were undertaken with a large scale rig incorporating a 1 x 1 x 1 m tank, filled with ~ 800 litres of water, and a jet-line of 15 mm internal diameter. The jet was driven by centrifugal pumps, allowing higher jet-tip velocities from 1.85 – 7.1 m/s. In the larger scale rig, the jet height was set to 10 diameters from the sediment bed interface, which parallels more closely conditions within the HASTs. The sediment bed itself was ~60 mm thick and at very high jet velocities the bed was again completely cleared from underneath the jet zone. As with the smaller rigs, the jet was left to run until a steady-state profile had been established for a given velocity, which normally occurred within 3 – 5 minutes, largely consistent with the small scale rig. The crater diameters and depths were established using the Ultrasonic Velocity Profiler (see following section).

The different studies conducted are summarised in Table 2, which lists a comparison of tested experimental variables and rig dimensions, for the three different jet and tank systems. It is noted that the pipe flow Reynolds numbers through both diameter jets are within the fully developed turbulent regime (> 4000) over the whole velocity range tested, and thus should have consistent expansion dynamics, apart from the very lowest velocity tested with the 3 mm jet system. At this velocity of 0.8 m/s, the corresponding Reynolds number is within the transitional regime, and may imply a reduced erosion potential, due to the lower turbulence levels.

2.3 Using an Ultrasonic Velocity Profiler (UVP) to study erosion

Both erosion kinetics and large-scale crater profiles were measured using a UVP-DUO ultrasonic velocity profiler (UVP) from Met-Flow (Switzerland). The UVP uses the associated Doppler frequency shift of transmitted acoustic pulse echoes, to establish the velocity of particles in the flow, as well described in literature (Thorne and Hanes, 2002). It also measures the strength of the backscattered echo at different depths to gauge the presence of solid surfaces. It consists of a small 2 MHz transducer head (active diameter 5 mm) connected via cables to a controller box and computer data logger. The Doppler frequency shift of the backscatter echo scattered off any particulates in the suspension is quantitatively converted to velocity values by the device. By assuming the speed of sound through the fluid (taken as that of water, 1485 m/s) the echo time-steps can be discretised into distance-steps, giving the ability to profile a full vertical distance range from the transducer head to the sediment bed. For all experiments the UVP was pulsed at 128 Hz (and a burst length of four cycles) where the echo responses were averaged at a sample rate of 500 ms. Given the moderate total distances, a 128 Hz pulse rate was deemed high enough to maximise data collection without leading to interferences from multiple pulse scatterings, which may occur at higher frequencies. A relatively high potential of 150 V was used, due to the possibility of acoustic attenuation through any suspended sand dispersion.

The UVP was employed in two ways. Firstly, it was used as a bed scanner to measure the steady-state profiles of the large-scale erosion craters. To do this, an automatic traverse was employed, with the UVP head being attached to it facing vertically down to the centreline of the crater about 150 mm above the bed. The UVP was set to record the echo signal in 1.1 mm discretised depth ‘bins’ for a total distance of 220 mm (which was therefore just beyond the glass bottom). A 1.1 mm bin size was used, to balance the requirements for accuracy with the necessity for it to be larger than single sand grains. The traverse then scanned the UVP probe across the crater from the near centre (at a speed of 1 mm/s) while the UVP continuously recorded velocity data for 5 minutes (Due to the

presence of the jet-line, the probe head was initially placed at a 23 mm off-set to the crater centre). This time based data was converted to distance, using the given traverse speed, correlating velocity data for a total length of 300 mm across the crater radius. A programme developed in MATLAB^{TM} allowed the measurement of the crater interface by the binary quantification of the velocity values, at the distance between a clear zero velocity value (being the static bed interface) and the non-zero value of the fluid above.

A defined threshold velocity level (normally 2 – 3 mm/s) was used as a basis to set the interface, where any bin values below this threshold were listed as '0' and any values above this listed as '1', for a given distance. Due to the potential for erroneous zero velocity values within the liquid above the interface (as the jet was disengaged, relative liquid movement was low) a further qualification of a standard error < 0.1 was required for a '0' binary value (it was assumed that relative error within the bed would be low). Then, the interface position was derived by outputting the first non-zero value, working back from the furthest distance from the probe. A five sample rolling average was used to help smooth outputted interface scans. Previous binary quantification of UVP signals has been used by the present authors (Hunter et al., 2011b) to measure the build-up and compression of consolidated beds from settling coagulated dispersions. A schematic of this set-up is shown in Fig. 2A. It is noted also that crater profiles were scanned in static conditions with the jet turned off, to better correlate data to the small-scale systems.

Secondly, the UVP was used to understand the kinetics of erosion, using the 0.5 m^3 rig and 3 mm jet-line. Here, the probe head was placed on an angle (of 68 degrees to the horizontal) and pointed towards the middle of the jet at the jet-bed interface, placed at a total distance of around 220 mm from the glass bottom. The UVP probe remained stationary and was set to record the velocity profiles of the flow again in 1.1 mm discretised depth 'bins' with a total distance of 200 bins (along the distance slice observable by the probe) for particular jet conditions over 2 minute runs (with the jet height set at 70 diameters). Additionally, the backscatter echo was measured, as it was assumed that any signal peaks may indicate the presence of the bed interface. Fig. 2B shows a schematic of these details (the probe's 'line of sight' is indicated by the dashed line in the figure). Hence, these measurements allowed assessment of changes to the true dynamic bed depths with time. The distance from the transducer head to the bed was also large enough to reduce any problems with flow disruption from associated intrusion into the jet-field.

One restriction of this set-up was that once erosion commenced, the 'line of sight' of the probe was no longer directly positioned at the jet-bed interface, but at a slight depth off-set to the centre. Given

the relatively high probe angle and moderate total bed depths (of 40 – 50 mm) this equated to a maximum centreline off-set (for a bed completely eroded to the tank floor) of ~ 19 mm. This off-set is also schematically shown in Fig. 2B. Nevertheless, this was determined to be acceptable due to the relatively flat nature of most cohesionless beds within the central region, and the comparatively small size of this off-set in relation to total crater sizes; although such positioning may be an issue for analysis of cohesive bed systems, where crater profiles are often comparatively deeper and narrower. Also the probe could not be positioned vertically, because of the necessity to take measurements while the jet was running.

3 Results & discussion

3.1 Influence of jet height & velocity

The effect of altering jet height on the erosion of sand systems was studied for heights between 30 mm and 400 mm (10d and 130d, where d is the jet diameter) in the small-scale rig. Experiments were conducted with average jet-tip velocities of between 1.44 - 5 m/s. Final measured steady-state crater depths and diameters are compared in Fig. 3. It is noted again that the jet was turned off before depth measurements were taken, and so they represent the static bed levels.

Firstly, it is observed that in respect of the change in crater depth with jet height (Fig. 3 A), a clear peak forms at intermediate levels (120 – 210 mm or 40d – 70d) with the maximum occurring at greater jet heights for increased velocities. This trend aligns well with previous studies into erosion behaviour with liquid jets (Aderibigbe and Rajaratnam, 1996; Kobus et al., 1979; Qi et al., 2000) and is linked to the balance between the jet-bed interaction velocity and total entrained jet volume at the bed interface. Although lifting the jet higher above the bed interface will lead to lower shear velocities in the impingement zone, as liquid entrains into the turbulent jet, its overall volume and thus interaction area with the bed will increase. The free-jet above the impingement zone will continue to entrain more liquid as it is raised further off the bed in a self-similar manner, which correspondingly will continue to reduce the overall impact velocities with the bed (Rajaratnam, 1976; Rushton, 1980). At some point, the impact velocities will be insufficient to create a critical shear stress required to erode the bed particles, and overall erosion will reduce. The jet height related to this peak will also correspondingly increase with the initial jet velocity, as is observed. Indeed for the lowest velocity, no distinguishable erosion occurred for any height greater than 210 mm (70d). This trend also has some important implications for the erosion efficiency in the nuclear HASTs. In this situation, the jets have been designed to be close to the tank base (at ~ 10d) to enhance the shear-velocities in the bed, but correspondingly, the small jet volume will likely reduce potential erosion in these systems.

Similar behaviour is evidenced in terms of the final steady-state diameters (Fig. 3 B). Here though, there appears to be a 'shoulder' in the general trends as the jet height is increased, and a very broad peak range. The reason for this broadening is that the crater profiles became distinctly flatter at very large jet heights, with ill-defined crater peaks. Although the measured depths and thus overall eroded volume was low, the very large jet interaction area with the bed created larger area impressions in the sediment. At the uppermost jet heights, the crater profiles were so indistinct that such measurements of size became very poor guides as to the true erosion potential of the jet.

The effect of altering jet velocities and sediment type was observed with the sand and both magnesium hydroxide distributions for set jet heights of 10d and 40d (with average jet-tip velocities varied between 0.8 – 4 m/s). Additionally, the potential for the jet to segregate species was investigated by measuring the erosion of a 50/50 v/v mix of the sand and coarse magnesium hydroxide. These results are shown collectively in Fig. 4.

Firstly, the influence of jet velocity on crater depth is discussed (Fig. 4, A1 & A2). At 10d, the sand and fine magnesium hydroxide show an increase in crater depth with velocity, as would perhaps be expected, with depths of the sand craters being slightly greater than the magnesium hydroxide, in line with the sand's smaller size. A distinct change in behaviour is observed for the coarse magnesium hydroxide however. Here, a clear peak occurs in the crater depths at intermediate jet velocities and, contrary to expectations, further increases in flow velocity above these intermediate levels reduce the crater depth.

The reasons for this phenomenon may be explained by the tendency for the jet to erode such large particulates in two distinct phases. Both Aderibigbe and Rajaratnam (1996) and Kobus et al. (1979) in sand studies determined two general interaction regimes (although Aderibigbe and Rajaratnam expanded this into two further sub-regimes). At low jet velocities, the jet's penetration into the bed in the impingement zone will be low, with erosion occurring via surface attrition that increases with jet velocity, with particulates being ejected outward in a radial profile with the bed (Type 1 erosion). However, at a certain velocity, the jet's penetration through the bed in the impingement zone is great enough to create a turbulent recirculation of the flow and thus bed materials (Type 2 erosion). This in turn initially creates a reduced crater depth once the jet is disengaged, due to the collapse of the recirculation effectively re-filling the crater. It is hypothesised that even for the smallest jet velocities studied, the sand and fine magnesium hydroxide only erode in a Type 2 manner (due to their small size) while the large magnesium hydroxide exhibits both interaction

types depending on the jet velocity. The erosion peak potentially occurs at the point where turbulent recirculation begins to develop. It is noted that at even higher velocities, as the turbulent recirculation zone expands, crater depths should continue to increase once more (as evidenced by the increase in measured bed depths of the sand and fine magnesium hydroxide).

At a height of 40d, a clear peak is evidenced in the steady-state static depths for both the coarse and fine magnesium hydroxide in this instance. At this greater jet height, overall jet-bed interaction velocities will be lower than at a height of 10d, but the interaction area will be increased. Such system changes (notably the reduced interaction velocities) result in conditions that now lead to intermediate size particulates such as the fine magnesium hydroxide also eroding in both regime types.

Final steady-state diameters for the three different sediment types (Fig. 4, B1 & B2) follow the expected trends for single particle cohesionless erosion. Here, the final diameters are consistently greater for the sand sediment, correlating to its small size distribution, while diameters for the fine magnesium hydroxide are slightly reduced in relation, due to its larger size. The coarse magnesium hydroxide, being almost five times as large as the sand sediment, has correspondingly significantly smaller crater diameters for a given jet velocity.

There are also some interesting differences in the erosion of sediment mixtures, observed in both the depth and crater size results displayed in Fig. 4. The erosion of 50% mixtures of sand and coarse magnesium hydroxide appears to lead to behaviour that approximately corresponds to the pure magnesium hydroxide alone. In other words, the erodibility of the bed is being highly damped by the partial mixture of the larger sediment. It seems that the jet is winnowing the fines by preferentially transporting them, resulting in a relatively coarse upper layer that armours the bed (Yeh et al., 2009). This also has some implications for the HAST systems, as it is known that there are a number of fission particulates present with varying size (McArthur et al., 2005; Paul et al., 2012) and these results imply the bed erodibility could be severely damped if similar segregation is taking place.

3.2 UVP measurement of large scale crater profiles

Crater profiles from eroded sand beds, using the large 1 m^3 tank rig and a 15 mm diameter jet-line, were measured using the UVP traverse system (Fig. 5), for jet-tip velocities between 1.86 m/s and 7.1 m/s, with the profiles shown in relation to the tank base (given as a zero depth). The dotted line indicates the original level of the sediment bed in the tank (at around 60 mm). The scanned profiles

generated from the binary quantification of the measured velocity values around the bed interface were also compared to photographed images for visual comparison of size, and results are shown together in Fig. 5. Again it is noted that in these studies that the jet was disengaged before the traverse measurements were taken, and so represent static crater profiles.

As observed from Fig. 5A, the MATLAB^{TM} protocol used to detect the bed interface worked well to quantify the steady-state profiles, for the range of jet velocities tested. Generally, the profiles suggest craters increase in both depth and size with jet velocity again in line with expectations for cohesionless materials. Here, erosion occurs via single particle momentum balance from the jet (Hogg et al., 1997; Mazurek and Hossain, 2007). As jet velocities increase, both the compressional pressure forces and lateral shear forces increase. Together, this leads not only to an increase in crater depth and size (as one might expect) but to increased peak crater heights (the peak height for the 1.86 m/s jet is around 83 mm, while for a jet velocity of 7.1 m/s it is ~ 100 mm). Similar changes have been measured by Yeh et al. (2009), using a laser scanning system and traverse. The overall measured crater radii (taken from the peak in the profiles) also compare favourably to the values taken from image analysis for clarification (see Fig. 5B).

One other important aspect to consider is the resolution of the UVP. Due to the sample time (of 500 ms, relating to 0.5 mm lateral distance) and the fact that a 5 point rolling average was used, there is an absolute minimum lateral-scan resolution of ~2.5 mm; though as a rolling and not an unqualified average was employed, in reality the sample resolution will tend to be higher than this. Furthermore however, acoustic transducers exhibit wave spreading from the focal point. The stated spreading half angle for these probes is 2.7^{o}, and for a total vertical beam distance of 20 cm this equates to a beam spread diameter of ~ 18 mm. Although echo responses will be distributed around the beam centreline, and this spread diameter represents itself more in a loss of signal strength, it indicates a lateral area of focus uncertainty. Additionally, due to the way echo profiles are discretised into bins, there is a minimum height resolution of +/- 1.1 mm (1 distance bin). Nevertheless, the well defined crater profiles produced from the scans (shown in Fig. 5) proved such resolution was in acceptable limits, although it may not be as high as some laser based scanning methods. However, these results are not only important for the analysis of cohesionless sediment erosion, but highlight the instrument's capability to profile fine cohesive erosion. In such fine particle systems, dispersion of the bed medium can cause the bulk fluid to become increasingly opaque, where subsequent settling and clarification occurs on such long time scales as to render visual analysis techniques (such as laser scanning (Yeh et al., 2009)) unusable. Indeed, future work will be conducted using an array of

probes to measure the crater profiles of cohesive sediment beds which more accurately simulate finer highly active nuclear waste fission products.

3.3 Normalised erosion data

Because the sand and magnesium hydroxide sediments were assumed to erode in a cohesionless manner, their erosion was normalised as considered by Rajaratnam and co-workers (Aderibigbe and Rajaratnam, 1996, 1998). This method relies on calculation of what is known as the erosion parameter 'E_c', given in Equation 1. Essentially, it is an association of the particle Froude number, where the jet tip velocity (U_0) is normalised with respects to the jet diameter (d) over the jet height (h) divided by a function of the particle fluid, incorporating the particle diameter (D) and the difference in density between the fluid and particle ($\Delta\rho/\rho_f$) as well as the gravitational constant (g).

$$E_c = \frac{U_o(d/h)}{\sqrt{gD\frac{\Delta\rho}{\rho_f}}} \qquad \text{Equation 1}$$

Therefore, any jet height-velocity combination will have an attributed E_c value, and different scale systems can be directly compared. It is noted that the D_{90} and not the D_{50} particle diameters were used as the average in this analysis, as it has been shown to give better representation due to the larger size fractions dominating bed erodibility in cohesionless systems (Aderibigbe and Rajaratnam, 1998; Yeh et al., 2009).

Fig. 6 shows the comparison between the final static depths (normalised over the jet height) of the sand, coarse and fine magnesium hydroxide in respect to increasing E_c numbers. Here, only the low to medium jet-velocity data are shown (corresponding to $E_c < 3$) to highlight differences between the species. It is clear from Fig. 6 that the three sediments do not normalise with each other (collapse onto a single relationship curve) however resulting trends within individual sediments are relatively consistent. A key reason for the differences in behaviour between sediments is likely due to the two phase jet-bed interaction regimes, which was linked to an interesting decrease in steady-state bed depth with increased jet velocity for the magnesium hydroxide sediments in some cases (as discussed in regards to Fig. 4). Both the coarse and fine magnesium hydroxide show a peak in the normalised depths at low E_c values, with the depth secondarily increasing at very high jet velocities (high E_c values). This again emphasises the complex dynamics between the jet and sediment bed at different jet heights and corresponding velocities. At low velocities, there is surface

attrition of particulates with the jet having low penetration, which increases initially with jet velocity. As velocity is increased over a certain threshold however, the deflected jet flow leads to a recirculation of particulates and fluid within the impingement zone. This correspondingly results initially in a reduction in, or stagnation to, measured static bed depths. At higher velocities the particles are expelled into larger recirculation zones and the normalised bed depths expand once more.

Kobus et al. (1979) showed similar evidence for the same type of two phase behaviour suggested by the hydroxide sediments in studies with sand, where the jet velocity was normalised with respects to the Stokes settling velocity of the particle (which gives a similar, although not identical correlation to normalising with respects to the E_c parameter). Again it is emphasised that this two regime behaviour is not actually evidenced with the sand in the current study, due to the relatively high interaction velocities and small sand size only leading to Type 2 (recirculating) erosion. This is highlighted in Fig. 6 with sand showing only a general trend of increasing depth with jet velocity (E_c values). In fact, Aderibigbe and Rajaratnam (1996) suggested turbulent recirculation would be created in sand systems for conditions where $E_c > \sim 0.35$. Given the small size of the sand, the lowest calculated E_c values in this study were only of the order of ~ 0.3, which approximately correlates with this boundary condition indicating only Type 2 erosion occurs.

More generally, some of the trend differences observed in Fig. 6 may be also related to particle shape or roughness effects that are not quantified in the normalisation routine shown in Equation 1. The jet's compressional pressure profile and resulting penetration through the bed will in particular be influenced by the bed's porosity and strength; and thus, even in well-defined cohesionless systems, will be dictated not only by particle size but also shape and roughness characteristics. Additionally, roughness can significantly affect the shear stress profile of the bed (Kobus et al., 1979) and the angle of incline of the formed craters. Microscopy images of the three sediment species (not shown) suggested that the coarse magnesium hydroxide in particular had an elongated shape profile and both hydroxide sediments had higher surface roughness than the sand. The complexity of trying to normalise for such a range of particle properties was deemed outside of the scope of the present study; however, future work is planned at categorising the angle of incline for a range of cohesionless and cohesive sediments using the UVP, to associate some of these additional parameters. Nevertheless, despite the limitations of the normalisation routine conducted, it was hoped that it may at least indicate some variations in performance between the three systems of different scales.

The effect of system scale was highlighted by comparing the normalised static sand crater depths from the small-scale rig, with results from the 0.5 m^3 scale and 1 m^3 (large scale) rigs, which are shown in Fig. 7. It is clearly observed that the small-scale normalised depths are relatively greater for a given E_c (or jet velocity). This is especially evident in regards to the large 1 m^3 scale rig, although unfortunately there was a relatively small velocity (E_c) range that both scale rigs were able to cover. Owing to air entrainment in the large scale pump rig, a minimum flow rate was required to produce a consistent jet, and consequently, there was limited scope to probe the lower jet velocity region (i.e. low E_c values). Likewise, the peristaltic pump used in the small and 0.5 m^3 rigs was unable to establish the high flow rate regime tested with the larger rig pump ($E_c > \sim 5$). Results with the 0.5 m^3 tank (using the same 3 mm jet line and pump system as the small rig) appear to be generally between the two extreme scales, although more closely aligned with the large scale. It is emphasised that, because data from all systems do not collapse onto the same overall curve when normalised, certain scale effects are partly defining the erosion potential of the system. This is critically important, as knowledge of what such effects may be, is required to gain an understanding of how well different systems may approximate potential erosion in the HASTs.

The literature trend shown in Fig. 7 (taken from (Aderibigbe and Rajaratnam, 1996)) seems to align more closely with the small-scale erosion test data. However, in our case, the small-scale data represent static crater depths (i.e. where the jet has stopped flowing) rather than a dynamic height (where the jet is still initiated) as in the case of the empirical literature relationship. It has been noted in a number of studies (Aderibigbe and Rajaratnam, 1996; Kobus et al. 1979; Al-Madhhachi et al., 2011), and also observed in the current results, that once the jet is disengaged, the crater partially refills as the recirculation settles, which reduces the overall depth in static conditions. Similar reductions in static bed measurements to the given literature trend were reported by Yeh et al. (2009), although the authors also suggested that the large jet diameter used and small studied jet heights may have contributed in this case. This again demonstrates the need for accurate active measurements of depth during jet operation.

Finally, the normalised crater size results are analysed in (Fig. 8), where the fine magnesium hydroxide, coarse magnesium hydroxide and sand from the small rig are compared to the sand data from the 0.5 m^3 and large scale rigs. The large 1 m^3 rig data represents size measurements for sand taken by both the UVP and visual image analysis, while all small-scale and 0.5 m^3 rig normalised data is from taken image analysis only. Here, crater sizes of the different sediment and tank systems were normalised by comparing the radius to the crater peak (r_1), over the jet-height. Firstly, it is observed that all the size data taken on the small-scale rig for the sand, fine and coarse magnesium

hydroxide appear to correlate far more closely together than the normalised depths, and approximately collapse onto a single relationship curve. This indicates that all the species are indeed eroding in a similar cohesionless manner and that additionally, the differences seen in the crater depths due to variations in jet-bed interaction do not lead to major changes in overall crater sizes. This would perhaps be expected, as the overall sizes are more dictated by shear movement of particles due to interactions with the jet in the low-velocity radial zone outside of the impingement area. Hence, differences in recirculation interaction underneath the jet in the impingement area will not influence the overall sizes to a high degree. It is clearly evident also in Fig. 8 that system scale has a significant influence on erosion (similar to the depth results shown in Fig. 7). As with the normalised depths, the crater sizes are relatively higher for sand from the small scale rig and reduce markedly for the large 1 m scale. Again, results with the 0.5 m^3 size rig (using the 3 mm jet line) lie somewhere between the two extremes, but much more closely align with the large scale data.

It is lastly noted that the given literature trend by Aderibigbe and Rajaratnam (1996) appears to be generally lower than the current data. The reason for the discrepancy in this case is likely due to different definitions of crater radius. Aderibigbe and Rajaratnam (1996) defined the radius to the original bed level (denoted as 'r_0'), while the radius to the crater peak (r_1) was measured in the present case, which correspondingly should lead to larger normalised sizes, as observed in Fig. 8. Analysis of r_0 was not possible in measurements where the Image J analysis technique was employed, as the original bed level could not be identified in formed craters from the top-down images. Nonetheless, r_0 was calculated for the large scale crater scans taken by the UVP, and the normalised data using these values are also shown in Fig. 8 (black cross symbols). Interestingly, it appears now that the literature trend over predicts the crater sizes using the r_0 data. We believe the reason for this discrepancy may be in the relatively small jet-height and high jet velocities employed in the large-scale rig. Again, Yeh et al. (2009) in similar low jet-height studies of sand erosion, found the same literature trend over-predicted measured sizes, and gave a calculated correction factor of 0.78. For the current r_0 UVP results as shown, the average correction factor needed to reduce the literature trend was calculated as 0.76, and is thus very consistent with this previous study.

It is important to consider why the small-scale system generally appears to lead to enhanced erosion. One potential reason may have been the use of a peristaltic pump in the small scale rig producing a pulsating jet generating increased erosion. However, it was thought that the relatively low magnitude and high velocity of the oscillations from the 'roller' type peristaltic action should not lead to significant pulsation, and the fact that erosion was reduced in the 0.5 m^3 tank (where the

same pump was used) suggested this was not a major concern. It was therefore thought instead that these changes were possibly associated with wall effects and different recirculation patterns created in each tank, which can interfere with the jet-bed interactions. The effect of system scale can be addressed by comparing two potentially important dimensionless length scales that may affect flow patterns within the tank. Firstly, the influence of lateral area constraints on jet behaviour is given by J_1 in Equation 2, where d again is the jet diameter and A the cross-sectional area of the tank.

$$J_1 = \frac{\pi(d/2)^2}{A} \qquad \text{Equation 2}$$

Secondly, the influence of tank volume in comparison to the jet flow discharge is given by J_2 in Equation 3, where additionally, U_0 represents the jet discharge velocity, H is the fluid depth within the tank and t is the jet-firing time. J_2 is thus a ratio of input jet volume for a given firing time to the ambient volume of the tank, and will vary as a function of input flow rate.

$$J_2 = \frac{U_o \pi(d/2)^2 t}{AH} \qquad \text{Equation 3}$$

These two numbers bear similarities with dimensionless numbers introduced in other fluid flow problems where tank size has been identified as an issue (Ross et al., 2011). The calculations of these size ratios for each tank and jet system used are given in Table 2. It is noted that U_0 = 5.2 m/s was used to estimate J_2, being the maximum jet-tip velocity tested with the 3 mm jet line in the small tank, and so represents the largest J_2 value. The firing time used in calculations was taken as 120 seconds.

Overall, the lateral area constraint (J_1) for the small rig with 3 mm jet and large 1 m^3 tank with 15 mm jet are similar, and in fact, is slightly less for the small scale rig, suggesting both tank sizes are large enough to reduce any interference from tank walls with the expanding radial jets. However, the total liquid volume contained in the large 1 m^3 rig is proportionally much greater because of the cylindrical nature of the small tank, which results in the calculated J_2 value being more than twice as big in the small-scale rig in comparison to the large tank. This increased unit discharge to volume ratio suggests that recirculation effects may be enhanced in the small-scale rig, due to the relatively smaller body of water in the tank to dissipate the jet's momentum. If such recirculation currents develop, this may also lead to greater levels of system turbulence, thereby amplifying the erosion in the system. Hence, it appears that the small-scale system is intensifying the jet's erosion potential.

The results with the 0.5 m^3 tank and 3 mm jet-line correlate well with this argument. In this case, both the lateral area ratio (J_1) and the unit discharge to volume ratio (J_2) are much smaller than the small-scale rig, considering especially that the same size jet line was used. Hence, problems of enhanced recirculation should be minimised, and correspondingly as evidenced in Fig. 7 and Fig. 8, overall erosion reduces to more closely align with normalised data from the large-scale rig.

3.4 UVP study of erosion kinetics

To study the flow velocities and kinetic depth changes associated with the erosion process, a series of trials were conducted with a jet height of 70 diameters (which correlated approximately with maximum bed erosion) and different flow velocities in the 0.5 m^3 scale rig (using the 3 mm jet-line). Fig. 9 shows the UVP 'colour-plots' associated with runs at 3.56 m/s (A) and 5 m/s (B). These plots display the internally averaged velocity values for each distance bin of a particular sample, and how these values change with time. In the resulting plots, colour bands are used to indicate velocity magnitude and sign, where green colours indicate velocity values away from the transducer (negative as given) and yellow/red colours particles moving towards the transducer (positive). Black areas indicate averaged velocities of zero to +/- 2 mm/s (the input threshold level). Schematics have been inserted to help detail some of the general trends highlighted by the colour plots, and it is important to note that the figures each represent a single distance slice, where the line of sight is indicated by the dashed black line in the schematic inserts. Also, because the colour-plots are produced by internal calibration with the UVP-DUO software, they do not contain an analysis of the standard deviation of the outputted values. Hence, it is difficult to quantify associated errors and thus the accuracy of these plots directly.

Nevertheless, a number of important features of the erosion process can be observed from the colour plots. Firstly in Fig. 9A, as the jet is initiated, the dynamic bed interface can be seen, from the zero velocity (black) ridge moving down the figure diagonally. The green region that increases in area above this with time arises from the jet-flow in the region immediately above the impingement, while the yellow regions above and below the dynamic bed represent particles being ejected out of the impingement zone and deflected towards the probe. By tracking the bed interface observable in the image, it suggests that the profile depth reaches a dynamic steady-state after a period of around 20 – 25 seconds (taking into account that the jet was initiated after 10 s). At the higher velocity (Fig. 9B) the bed interface is also seen in the image from the black ridge, but here a steady-state state is established rapidly, within 10 seconds. It is noted that at this velocity, the sediment bed was completely cleared from underneath the jet, and the final depth (being equal to the tank base) was just beyond the distance measured by the UVP. Only the green zone representing

the jet velocities above impingement can be seen, as a band at the base of the image. Additionally with the higher velocity, the greater jet-bed interaction causes the fluid to deflect into a larger and more turbulent recirculation zone. This behaviour caused a distinct suspension cloud-front to form above the jet. This was both evidenced visually and can be seen in the colour plot as the upper interface zone between particles flowing towards the transducer (red to yellow zone) and cycling back down into the jet region (upper green zone). Indeed, similar enhanced recirculation has previously been shown by Aderibigbe and Rajaratnam (1996) for very high velocity jets.

In addition to the qualitative assessment available from the colour-plots, a further analysis was conducted that attempted to quantify these kinetic changes by measuring the distance position relating to the peak echo response. Initially, as in the scans of the static crater profiles, binary quantification was conducted of the velocity values in an attempt to highlight the sediment bed at the zero velocity boundaries. Unfortunately, as these systems had very fast dynamic changes and the bed itself was effectively constantly in motion, due to its ejection and recirculation, this method was found to be unstable for analysing such kinetics. In order to overcome this, a second approach was used. Here, the distance corresponding to the peak in the root-mean-square of the echo profile was measured for the region in the vicinity of the bed-suspension interface estimated from the colour plots (distances of 140 to 220 mm from the transducer). This peak was correlated to the sediment-bed, under the assumption that the interface would reflect a strong echo signal back to the probe (Rice et al., 2012).

The measured changes in the distance from the probe to the signal peak over time were converted to be in relation to the glass tank bottom (with 0 mm the tank bottom) and thus represented measured segmental bed thicknesses. As the probe head was at an angle (of 68^o to the horizontal) the vertical bed height was estimated from these results, by multiplying the measured segmental thickness by $\sin(68^o)$. The results of this analysis are shown in Fig. 10 for jet velocities of 2.43, 3.56 and 5 m/s, and represent the estimated vertical bed height changes over time (near the jet-centreline). Due to individual sample noise, the profiles shown represent a five-value rolling average, which equates to a maximum time resolution of 2.5 s.

It is noted that derived kinetic trends from the UVP must be made with some caution, due to the probe offset and the potential acoustic spreading. Again it is emphasized that the given estimated vertical depth essentially assumes there is a flat bed between the centre and the maximum distance off-set (of ~19 mm). Due to the large size of the craters (of between 15 and 20 cm, see Fig. 4) and the relatively flat aspect ratio of the cohesionless crater profiles, this assumption appears acceptable.

Additionally, as with the scanning UVP measurements, acoustic spreading means the recorded bed depths represent the mean from a maximum lateral area of ~18 mm (although again, the focus area will be much smaller than this) and any measured vertical distances will have an error of approximately +/- 1.1 mm (one distance bin). Nevertheless, it is also emphasized again that this angled set-up was necessary to observe kinetic changes in situ because of the position of the jet-line.

Despite these potential limitations of the angled acoustic technique, the kinetic changes to the eroded bed can be clearly seen from the measured change in sediment peak with time for the three conditions tested. For tests at 3.56 and 5 m/s (relating to conditions shown in Fig. 9) again the faster jet velocity results in more rapid erosion of the interface with time and complete clearance of the sand within 10 seconds, while the run at 3.56 m/s suggests a dynamic steady-state equilibrium is established in approximately 20 seconds after the jet is initiated (30 seconds total time as given). It is emphasised that this represents equilibrium of the central bed depth and not total crater size, as it would be expected that erosion in the outer radial jet region would continue after this time. For these two conditions, the jet was switched off after 80 seconds, where a critical and distinct rise in the bed height is observed in both cases. This rise relates to the bed refilling that occurs in static conditions, and it highlights how dramatic such changes may be for measured depth profiles. Such changes correlate with the normalised results given in Fig. 7, where the given literature trend of dynamic depths (Aderibigbe and Rajaratnam, 1996) was significantly above the static depths measured in this study.

In addition, it appears that there are large variations between the measured static and dynamic depths in relation to jet flow rate. The comparative differences in static bed depths observed in Fig. 10 for conditions at 3.56 and 5 m/s (at times after the jet is disengaged) are very minor. This correlates with static depth data shown in Fig. 4 and normalised data shown in Fig. 7, which indicated that above a flow rate of ~3-4 m/s, the change in sand depth is not significant and approaches an asymptotic value. However, the dynamic bed depth measured at 5 m/s shown in Fig. 10 is significantly greater than at 3.56 m/s. This is likely because at the higher velocity, a more pronounced turbulent recirculation zone will be created (as highlighted by the observations of a dispersion cloud-zone evidenced in the colour-plot in Fig. 9) and refilling upon jet disengagement will be much more significant. Such accurate quantification of the complex kinetic changes within the impingement zone are critical to a greater understanding of the erosion mechanism by turbulent liquid jets, and highlights the potential of such ultrasonic instrumentation to derive a level of information not previously accessible.

At the slowest jet velocity run shown in Fig. 10 (2.43 m/s) a noted decrease in the kinetic rate of erosion is evidenced, as perhaps would be expected given the reduced jet-bed interaction force. Additionally, a much greater time is required to reach dynamic steady-state (which appears to occur after approximately 100 seconds total time). Hence, the jet was run for 130 seconds before being switched off, where a similar but less distinct bed rise occurs due to the crater refilling. Therefore in general, as jet velocity is increased, not only does the initial kinetic rate of erosion increase along with the total amount eroded, but the time taken to reach steady-state is correspondingly reduced. This has important implications for the HAST systems, as due to limited liquid ballast fill volumes, a delicate balance exists between jet velocities and total jet firing times. Such results suggest that optimal conditions would be to operate at maximum attainable velocities, as the increased erosion rate and paralleled reduced time for steady-state to occur, would counterbalance the reduction in attainable firing times.

4 Conclusions

The work presented in this paper has helped establish the effect of system scale in studies of cohesionless sediment erosion by impinging vertical jets, to critically analyse the potential correlation of a laboratory scale rig to industrial ballast systems. Normalised crater depth and radii data suggest that the erosion was amplified in the small scale rig, perhaps due to increased turbulent recirculation currents. Two dimensionless numbers are introduced to aid quantification of the influence of system scale on jet impingement dynamics and erosion, based on consideration of jet to tank cross-sectional areas, and jet discharge to tank volume.

A novel methodology for measuring dynamic erosion in situ at unprecedented frequency-resolution was demonstrated using an ultrasonic Doppler velocimeter (UVP). The UVP enables the measurement of dynamic crater depths and profiles, erosion kinetics and steady-state timescales, and even jet flow-fields. More generally, the UVP has great potential to also measure erosion dynamics in pulsed systems and fine particle systems, due to its ability to penetrate optically opaque dispersions. Hence, it will be applicable to the study of a range of cohesive sediments that are important in a wide array of industries, and specifically more closely mirror species found within nuclear waste processing.

Acknowledgments

The authors would like to thank the EPSRC through the DIAMOND Consortium for funding this project. Thanks are also given to the National Nuclear Laboratory, Sellafield Ltd. and the Sorby Environmental Fluid Dynamics Laboratory for collaboration on this project. Lastly, thanks are

given to the two anonymous reviewers, for their perceptive comments that significantly improved this paper.

References

Aderibigbe, O.O., Rajaratnam, N., 1996. Erosion of loose beds by submerged circular impinging vertical turbulent jets. Journal of Hydraulic Research 34, 19-33.
Aderibigbe, O.O., Rajaratnam, N., 1998. Effect of sediment graduation on the erosion by plane turbulent wall jets. Journal of Hydraulic Engineering 124, 1034-1042
Al-Madhhachi, A.T., Hanson, G.J., Fox, G.A., Tyagi, A.K., Bulut, R., 2011. Measuring erodibility of cohesive soils using laboratory jet erosion tests, World Environmental and Water Resources Congress Palm Springs, USA, pp. 2350 - 2359.
Ansari, S.A., Kothyari, U.C., Raju, K.G.R., 2003. Influence of cohesion on scour under submerged circular vertical jets. Journal of Hydraulic Engineering 129, 1014-1019.
Baas, J.H., Best, J.L., Peakall, J., Wang, M., 2009. A phase diagram for turbulent, transitional, and laminar clay suspension flows. Journal of Sedimentary Research 79, 162–183.
Birkhofer, B.H., Jeelani, S.A.K., Windhab, E.J., Ouriev, B., Lisner, K.-J., Braun, P., Zeng, Y., 2008. Monitoring of fat crystallization process using UVP-PD technique. Flow Measurement and Instrumentation 19, 163-169.
Caruso, C., Gabr, M., 2011. In situ assessment of scour potential with depth using jetting approach. Geo-Frontiers Special Publication, 1483-1492.
Debnath, K., Nikora, V., Aberle, J., Westrich, B., Muste, M., 2007. Erosion of cohesive sediments: Resuspension, bed load and erosion patterns from field experiments. Journal of Hydraulic Engineering 133, 508-520.
Ein-Mozaffari, F., Bennington, C.P.J., Dumont, G.A., Buckingham, D., 2007. Measuring flow velocity in pulp suspension mixing using ultrasonic Doppler velocimetry. Chemical Engineering Research and Design 85, 591-597.
Ein-Mozaffari, F., Upreti, S.R., 2009. Using ultrasonic Doppler velocimetry and CFD modeling to investigate the mixing of non-Newtonian fluids possessing yield stress. Chemical Engineering Research and Design 87, 515-523.
Gioia, G., Bombardelli, F.A., 2005. Localized turbulent flows on scouring granular beds. Physical Review Letters 95, 014501/014501-014501/014504.
Hamm, B.A., West, W.L., Tatterson, G.B., 1989. Sludge suspension in waste storage tanks. AIChE Journal 35, 1391-1394.
Harbottle, D., Fairweather, M., Biggs, S., 2011. The minimum transport velocity of colloidal silica suspensions. Chemical Engineering Science 66, 2309-2316.
Hastings, J.J., Rhodes, D., Fellerman, A.S., McKendrick, D., Dixon, C., 2007. New approaches for sludge management in the nuclear industry. Powder Technology 174, 18-24.
Hogg, A.J., Huppert, H., E., Dade, W.B., 1997. Erosion by planar turbulent wall jets. Journal of Fluid Mechanics 338.
Hunter, T.N., Biggs, S.R., Young, J., Fairweather, M., Peakall, J., 2011a. Ultrasonic techniques for the in situ characterisation of 'Legacy' waste sludges & dispersions, ICEM Sep 25 - 29, Reims, France, 59111.
Hunter, T.N., Peakall, J., Biggs, S.R., 2011b. Ultrasonic velocimetry for the in situ characterisation of particulate settling and sedimentation. Minerals Engineering 24, 416-423.
Jain, R.K., Kothyari, U.C., 2009. Cohesion influences on erosion and bed load transport. Water Resources Research 45, W06410/06411-W06410/06417.
Kantoush, S.A., De Cesare, G., Boillat, J.L., Schleiss, A.J., 2008. Flow field investigation in a rectangular shallow reservoir using UVP, LSPIV and numerical modelling. Flow Measurement and Instrumentation 19, 139-144.
Karim, O.A., Ali, K.H.M., 2000. Prediction of flow patterns in local scour holes caused by turbulent water jets. Journal of Hydraulic Research 38, 279 - 287.
Kobus, H., Leister, P., Westrich, B., 1979. Flow field & scouring effects of steady and pulsating jets impinging on a movable bed. Journal of Hydraulic Research 17, 175-192.
Kotze, R., Wiklund, J., Haldenwang, R., Fester, V., 2011. Measurement and analysis of flow behaviour in complex geometries using the Ultrasonic Velocity Profiling (UVP) technique. Flow Measurement and Instrumentation 22, 110-119.
Mali, R.G., Patwardhan, A.W., 2009. Characterization of onset of entrainment in stirred tanks. Chemical Engineering Research and Design 87, 951-961.
Mazurek, K.A., Hossain, T., 2007. Scour by jets in cohesionless and cohesive soils. Canadian Journal of Civil Engineering 34, 744-751.

McArthur, G.A.H., Harken, J.P., Rawlinson, G., Woodhouse, G., Claxton, D., 2012. Further development of a liquid jet sludge re-suspension model, Nuclear Fuel Cycle Conference, April 23 - 25, Manchester.
McArthur, G.A.H., Tinsley, T.P., McKendrick, D., 2005. Development of a liquid jet sludge re-suspension model (used on pulse jets or jet ballasts), AIChE Annual Meeting, Conference Proceedings, Oct. 30-Nov. 4, Cincinnati, OH, United States, pp. 480a/481-480a/414.
Paul, N., Hammond, R., Biggs, S., Edmonson, M., 2012. Characterising highly active nuclear waste simulants, Nuclear Fuel Cycle Conference, April 23 - 25, Manchester.
Qi, M., Fujisak, K., Tanaka, K., 2000. Sediment re-suspension by turbulent jet in an intake pond. Journal of Hydraulic Research 38, 323 - 330.
Rajaratnam, N., 1976. Turbulent jets. Elsevier, Amsterdam.
Rajaratnam, N., 1982. Erosion by submerged circular jets. Journal of Hydraulics Division, ASCE 108, 262-267.
Rajaratnam, N., Beltaos, S., 1977. Erosion by impinging circular turbulent jets. Journal of Hydraulics Division, ASCE 103, 1191-1205.
Rajaratnam, N., Zhu, D.Z., Rai, S.P., 2010. Turbulence measurements in the impinging region of a circular jet. Canadian Journal of Civil Engineering 37, 782-786.
Rice, H., Hunter, T.N., Peakall, J., Biggs, S., Fairweather, M., 2012. Behaviour of time-dependent bedforms in closed pipe flow, Turbulence, Heat and Mass Transfer 7, Sep 24 - 27, Palermo, Sicily.
Ross, J.A., Peakall, J., Keevil, G.M., 2011. An integrated model of extrusive sand injectites in cohesionless sediments. Sedimentology 58, 1693-1715.
Rushton, J.H., 1980. The axial velocity of a submerged axially symmetrical fluid jet. AIChE Journal 26, 1038-1041.
Sequeiros, O.E., Nino, Y., Garcia, M.H., 2007. Erosion of finite thickness sediment beds by single and multiple circular jets. Journal of Hydraulic Engineering 133, 495-507.
Shekarriz, A., Hammad, J.K., 1997. Evaluation of scaling correlations for mobilization of double-shell tank waste. Pacific Northwest National Laboratory, Richmond, Washington
Shekarriz, A., Hammad, J.K., Powell, M.R., 1997. Research of jet mixing of settled sludges in nuclear waste tanks at Hanford and other DOE sites: A historical perspective. Pacific Northwest National Laboratory, Richmond, Washington.
Thorne, P.D., Hanes, D.M., 2002. A review of acoustic measurement of small-scale sediment processes. Continental Shelf Research 22, 603-632.
Tolhurst, T.J., Black, K.S., Paterson, D.M., 2009. Muddy sediment erosion: Insights from field studies. Journal of Hydraulic Engineering 135, 73-87.
Tolhurst, T.J., Black, K.S., Paterson, D.M., Mitchener, H.J., Termaat, G.R., Shayler, S.A., 2000. A comparison and measurement standardisation of four in situ devices for determining the erosion shear stress of intertidal sediments. Continental Shelf Research 20, 1397-1418.
Xue, W.-y., Huai, W.-x., Qian, Z.-d., 2010. Numerical simulation of sediment erosion by submerged plane turbulent jets. Journal of Hydrodynamics, Ser. B 22, 593-598.
Yeh, P.-H., Chang, K.-A., Henriksen, J., Edge, B., Chang, P., Silver, A., Vargas, A., 2009. Large-scale laboratory experiment on erosion of sand beds by moving circular vertical jets. Ocean Engineering 36, 248-255.

Figure Captions

Figure 1: Measured particle size distributions for sand, and fine and coarse magnesium hydroxide.

Figure 2: Schematics of UVP set-ups.

Figure 3: Changes to sand crater depths (A) and diameters (B) for different jet heights.

Figure 4: Changes to crater depths (A1 & 2) and diameters (B1 & 2) for sand, fine and coarse $Mg(OH)_2$ as well as a 50% v/v mixture of sand and coarse $Mg(OH)_2$, for various jet velocities at heights of 10*d* and 40*d*.

Figure 5: Large-scale static sand crater profiles measured by the UVP for various jet velocities (A) and images for visual comparison (B).

Figure 6: Crater depths/jet-height versus normalized erosion parameter 'E_c' for sand, fine and coarse $Mg(OH)_2$. Dashed lines represent 5 number rolling averages.

Figure 7: Comparison between normalized eroded sand depths for the small, 0.5 m^3 and large 1 m^3 scale rigs. The dashed-line empirical relationship is taken from Aderibigbe and Rajaratnam (1996).

Figure 8: Comparison of normalized crater radii for all sediments in the small scale rig to sand results from the 0.5 m^3 and 1 m^3 large scale rigs. The dashed-line represents the empirical relationship of Aderibigbe and Rajaratnam (1996).

Figure 9: UVP colour-plots of sand erosion for jet velocities at 3.56 m/s (A) and 5 m/s (B).

Figure 10: Erosion kinetics measured from UVP backscatter signal of the crater interface for jet velocities of 2.43, 3.56 and 5 m/s. Dashed lines represent a 5 number rolling average.

Table 1: D_{50} and D_{90} average sizes for the tested sediments.

Table 2: Comparison of experimental variables for the three different sized tank rigs.

Table 3: Jet-tank size ratio numbers J_1 and J_2 (defined with U_0 = 5.2 m/s and t = 120 s).

Figure 1

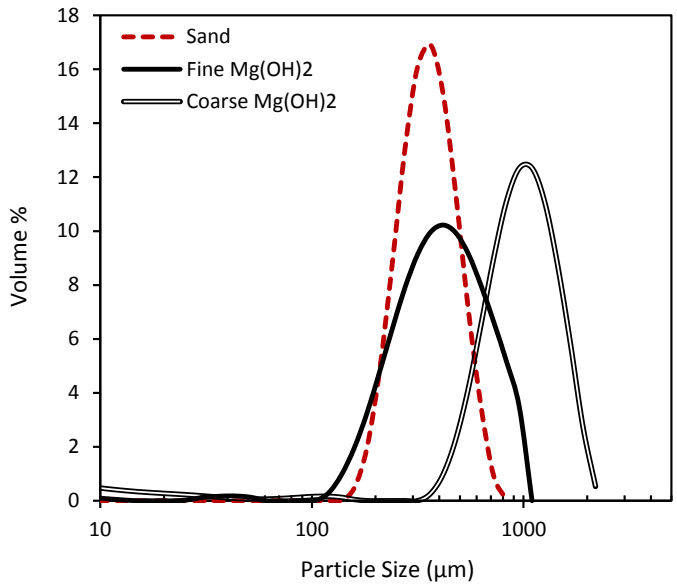
Sand
Fine Mg(OH)2
Coarse Mg(OH)2
Volume %
Particle Size (µm)
0
2
4
6
8
10
12
14
16
18
10
100
1000

Figure 2

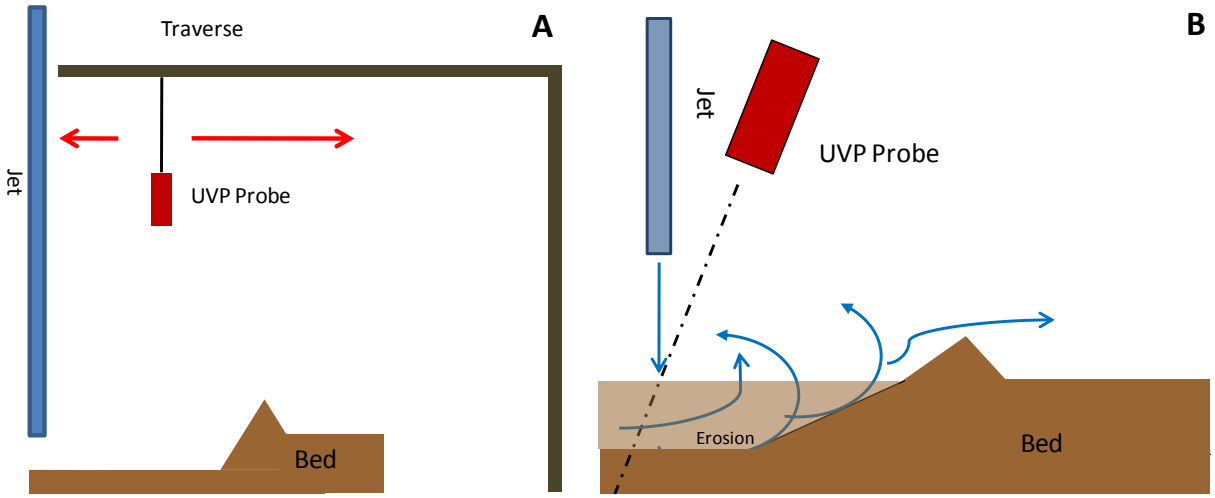

Figure 3

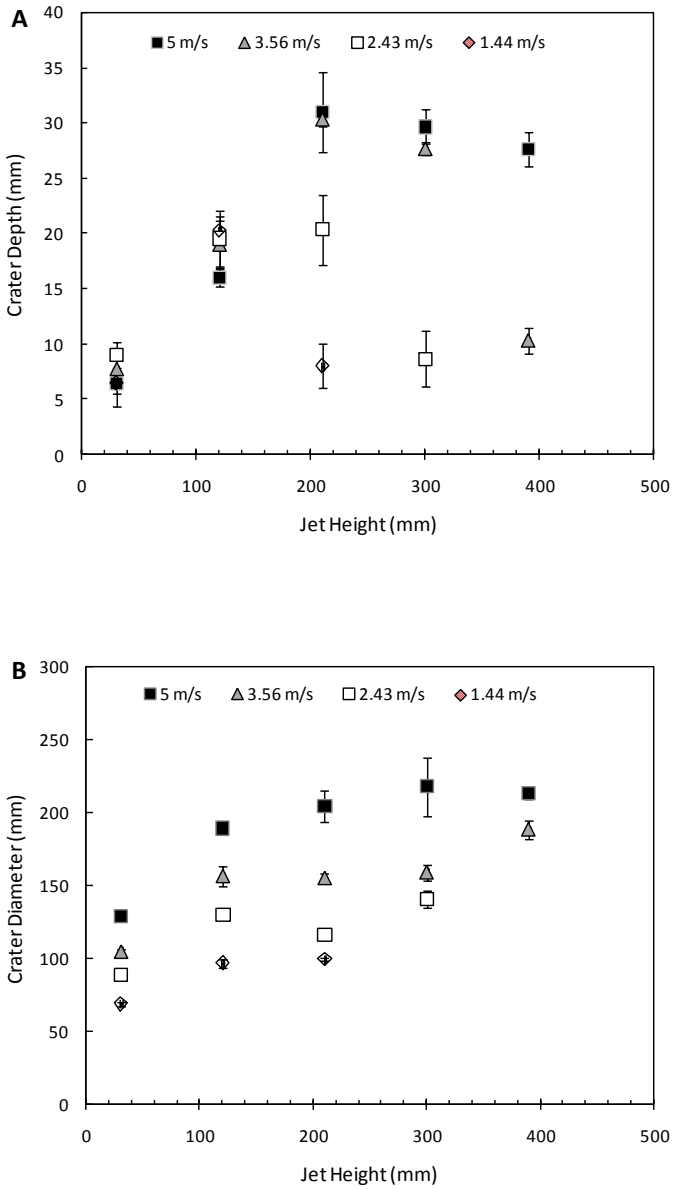
A
5 m/s
3.56 m/s
2.43 m/s
1.44 m/s
Crater Depth (mm)
Jet Height (mm)
0
5
10
15
20
25
30
35
40
0
100
200
300
400
500
B
5 m/s
3.56 m/s
2.43 m/s
1.44 m/s
Crater Diameter (mm)
Jet Height (mm)
0
50
100
150
200
250
300
0
100
200
300
400
500

Figure 4

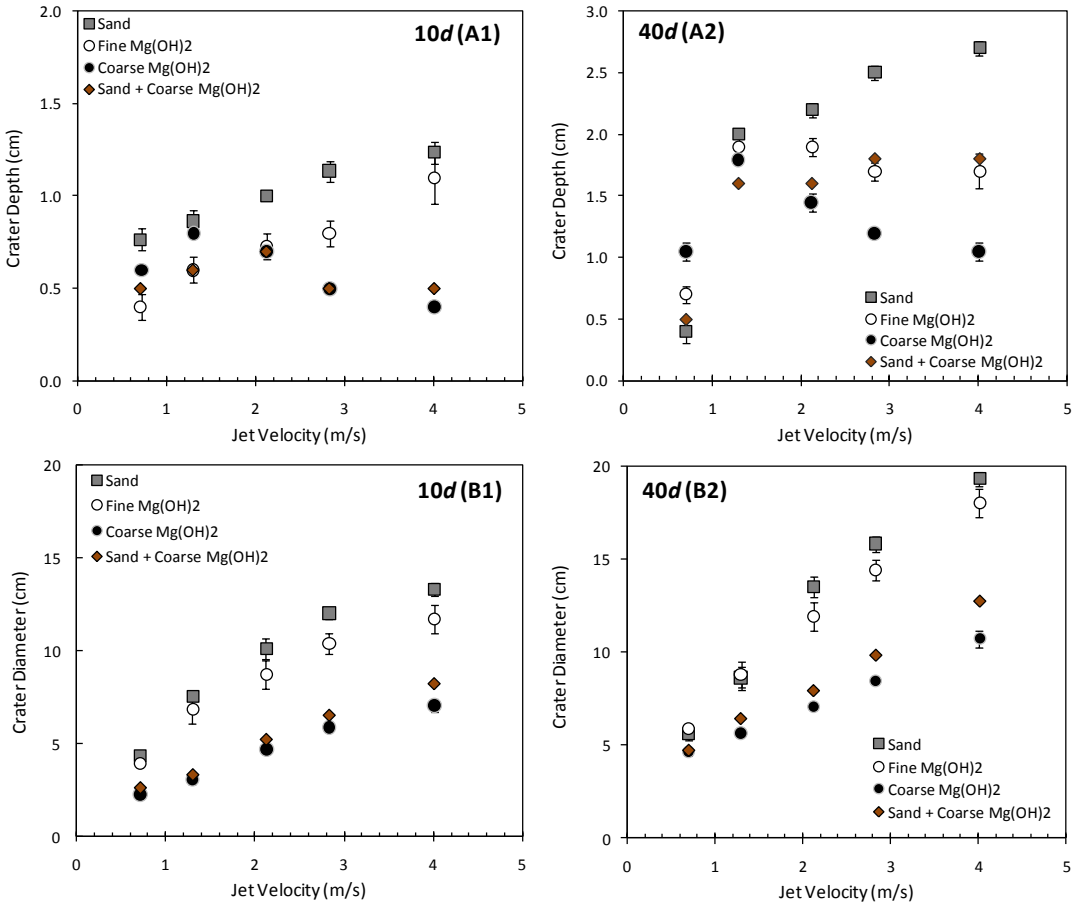
10d (A1)
40d (A2)
10d (B1)
40d (B2)
Sand
Fine Mg(OH)2
Coarse Mg(OH)2
Sand + Coarse Mg(OH)2
Crater Depth (cm)
Crater Diameter (cm)
Jet Velocity (m/s)

Figure 5

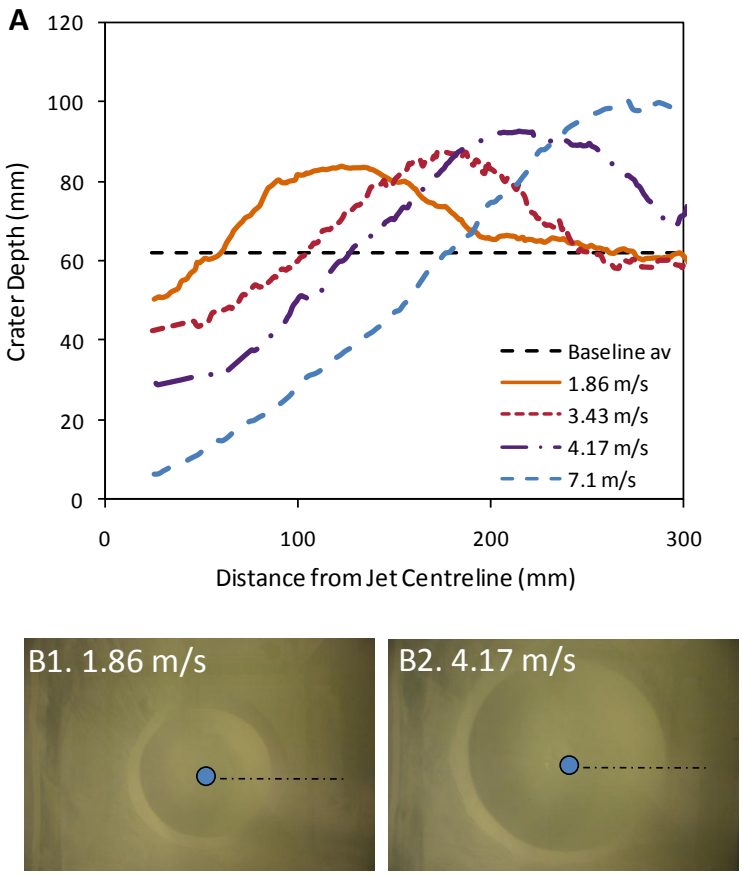
A
120
100
80
60
40
20
0
Crater Depth (mm)
0
100
200
300
Distance from Jet Centreline (mm)
Baseline av
1.86 m/s
3.43 m/s
4.17 m/s
7.1 m/s
B1. 1.86 m/s
B2. 4.17 m/s

Figure 6

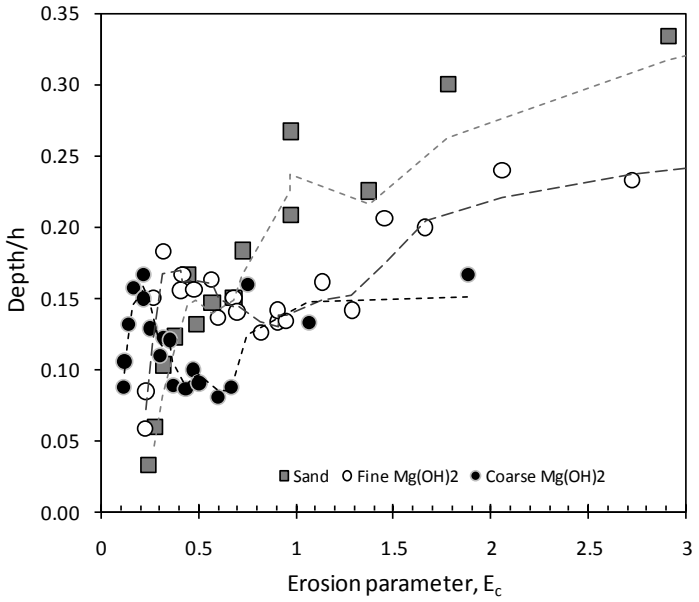
0.35
0.30
0.25
0.20
0.15
0.10
0.05
0.00
Depth/h
0
0.5
1
1.5
2
2.5
3
Erosion parameter, E_c
Sand
Fine Mg(OH)2
Coarse Mg(OH)2

Figure 7

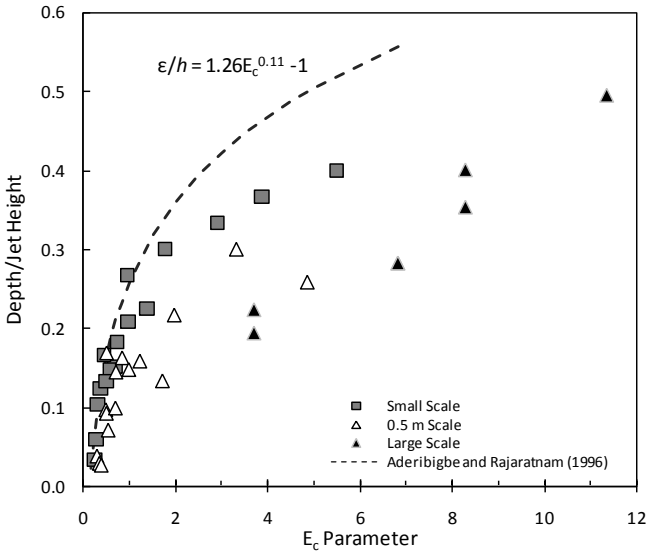
0.6
0.5
0.4
0.3
0.2
0.1
0.0
Depth/Jet Height
ε/h = 1.26E_c^0.11 -1
Small Scale
0.5 m Scale
Large Scale
Aderibigbe and Rajaratnam (1996)
0
2
4
6
8
10
12
E_c Parameter

Figure 8

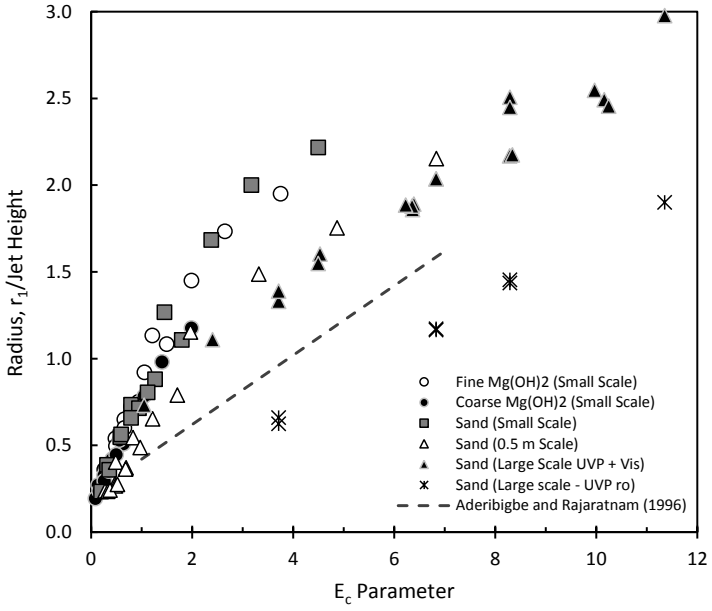
3.0
2.5
2.0
1.5
1.0
0.5
0.0
0
2
4
6
8
10
12
Radius, r1/Jet Height
Ec Parameter
Fine Mg(OH)2 (Small Scale)
Coarse Mg(OH)2 (Small Scale)
Sand (Small Scale)
Sand (0.5 m Scale)
Sand (Large Scale UVP + Vis)
Sand (Large scale - UVP ro)
Aderibigbe and Rajaratnam (1996)

Figure 9

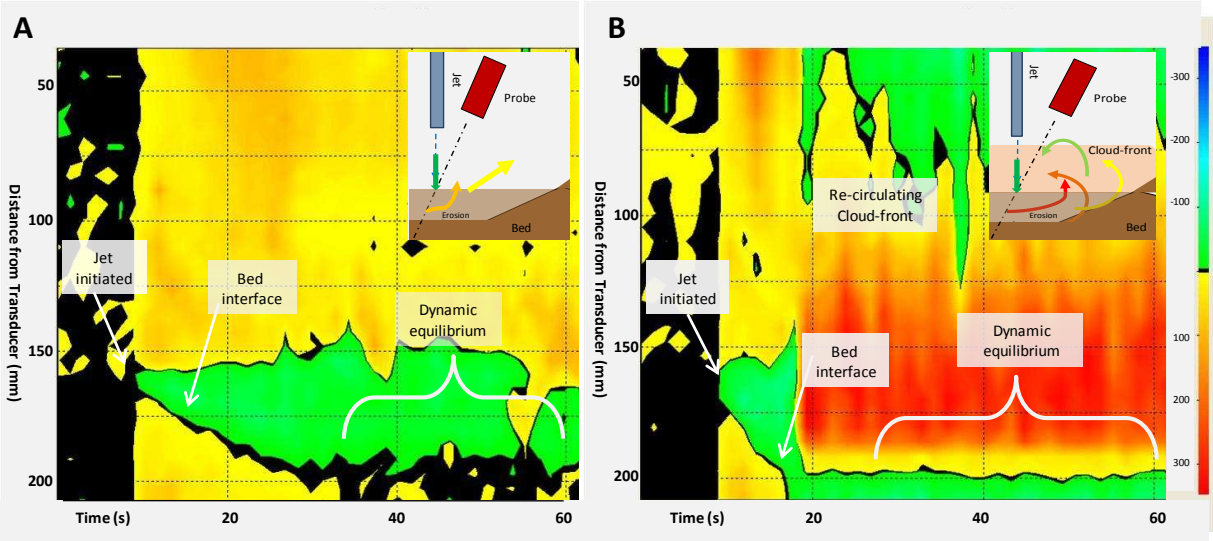
A
B
Distance from Transducer (mm)
Time (s)
50
100
150
200
20
40
60
Jet
Probe
Erosion
Bed
Cloud-front
Jet initiated
Bed interface
Dynamic equilibrium
Re-circulating Cloud-front
-300
-200
-100
100
200
300

Figure 10

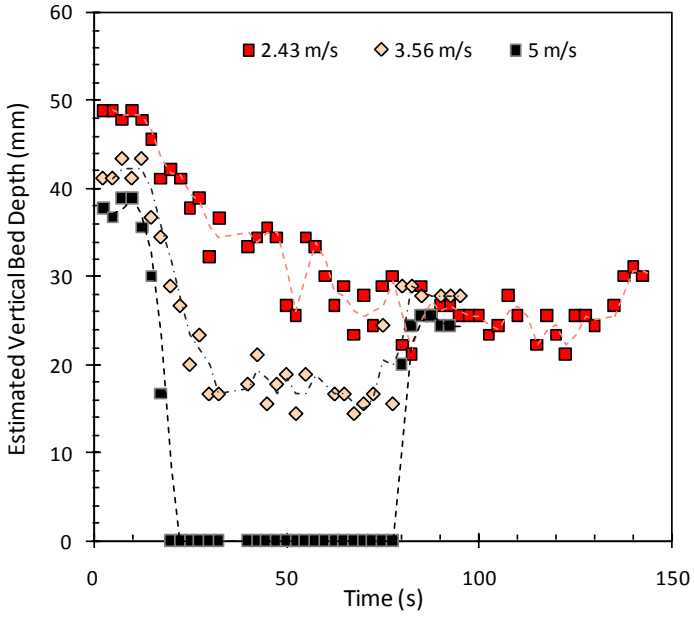
2.43 m/s
3.56 m/s
5 m/s
Estimated Vertical Bed Depth (mm)
Time (s)
0
10
20
30
40
50
60
0
50
100
150

Table 1

Table 1: D_{50} and D_{90} average sizes for tested cohesionless sediments.

Sediment	**D_{50} (µm)**	**D_{90} (µm)**
Sand	328	489
'fine' $Mg(OH)_2$	375	702
'Coarse' $Mg(OH)_2$	1400	2500

Table 2: Comparison of tested experimental variables for the three different sized tank rigs.

Variable	Small Cylinder Tank	Cubic Tank - 0.5 m^3	Cubic Tank - 1 m^3
Tank fill dimensions (mm)	0.28 (d_t), 0.4 (H)	0.5 (L), 0.5 (W), 0.4 (H)	1 (L), 1 (W), 0.8 (H)
Tank fill volume (L)	25	100	800
Jet diameter '*d*' (mm)	3	3	15
Jet heights	10*d* – 130*d*	10*d* – 70*d*	10*d*
Jet velocities (m/s)	0.8 – 5.2	0.8 – 5.2	1.85 – 7.1
Jet Reynolds Nos.	2,400 – 15,600	2,400 – 15,600	27,750 – 106,500
Sediments	Sand, 'Fine' $Mg(OH)_2$ & 'Coarse' $Mg(OH)_2$	Sand	Sand

Table 3: Jet-tank size ratio numbers J_1 and J_2 (definied with U_0 = 5.2 m/s and t = 120 s).

	3 mm Jet, Small Tank	3 mm Jet, 0.5 m^3 Tank	15 mm Jet, 1 m^3 Tank
J_1	1.15×10^{-4}	2.83×10^{-5}	1.77×10^{-4}
J_2	2.87×10^{-4}	4.41×10^{-5}	1.38×10^{-4}